Discrete focusing effect of positive ions by a plasma-sheath lens

E. Stamate and H. Sugai
Nagoya University, Department of Electrical Engineering and Computer Science, Furo-cho, Chikusa-ku, Nagoya 464-8603, Japan
(Received 13 May 2005; published 14 September 2005)

We demonstrate that the sheath created adjacent to the surface of a negatively biased electrode that interfaces an insulator acts as a lens that focuses the positive ions to distinct regions on the surface. Thus, the positive ion flux is discrete, leading to the formation of a passive surface, of no ion impact, near the edge and an active surface at the center. Trajectories of positive ions within the sheath are obtained by solving in three dimensions the Poisson equation for electrodes of different geometry. Simulations are confirmed by developing the ion flux profile on the electrode surface as the sputtering pattern produced by ion impact. Measurements are performed in a dc plasma produced in Ar gas.

DOI: 10.1103/PhysRevE.72.036407 PACS number(s): 52.25.−b, 52.27.−h

I. INTRODUCTION

The sheath is a space charge layer that forms to a biased electrode whenever $V_0 \neq V_{\mathrm{pl}}$, where V_0 is the applied bias and V_{pl} the plasma potential [1]. If $V_0 < V_{\mathrm{pl}}$ the electrode reflects electrons and accelerates ions resulting in distinct profiles of electron density, n_e, and positive ion density, n_i [2–6]. The sheath edge (plasma-presheath boundary), Σ, is usually defined as the location where the positive ion velocity equals the ion acoustic speed, c_s [7], so that Σ is the equipotential contour given by $V_{\mathrm{sh}}=kT_e/(2e)$, where T_e is the electron temperature. For an infinite planar electrode Σ is parallel to the surface and the sheath expands in front of the electrode to a length defined as the sheath thickness, D. In practice, the electrode is finite so that the surrounding sheath can only be described in two or three dimensions. The positive ion accumulates energy within the sheath then strike the surface with a certain incidence angle, α_{imp}, inducing surface modification. This scenario is common to most plasma processing technologies such as sputtering, etching, oxidation, or implantation, where one of the main requirements is to attain uniform treatment over the sample surface [8].

Special attention was devoted to the investigation of sheath profile and ion dose uniformity. Conrad [9] reported potential profiles for sheath surrounding cylindrical and spherical electrodes and Donnelly and Watterson [10,11] for complex and wedge shapes. Later, Hong and Emmert [12] and Sheridan [13] reported that the incident ion dose was peaked near to, but not on, the corner of a square bar during ion implantation. The two-dimensional simulation of expanding plasma sheath was reported by Paulus *et al.* [14]. In 1998, Fan *et al.* [15] reported sample stage-induced dose nonuniformity in plasma ion implantation of silicon. They explained the resulting effect by charging of the quartz shroud used to reduce contamination. However, similar profiles, with a sputtered ring and central spot, were reported by Stamate and Ohe [16,17] and have been associated with ion focusing by a sheath lens effect. Thus, the edge effect of a planar electrode induced an ellipticlike sheath structure that acted as an electrostatic lens focusing positive ions to distinct parts of the electrode surface. So far, this was the first experiment to demonstrate the discrete behavior of the ion flux, resulting in the formation of the passive surface (PS), near the edge, and active surface (AS), at the center. The application of the focusing effect to measure D and to detect the negative ion was also reported [18,19]. Later on, Tian and Chu [20] revised the result on stage-induced dose nonuniformity [15] also attributing the observed patterns to ion-focusing effects. Recently, several reports investigated the ion dynamic within the sheath surrounding targets with grooves [21] patterned surfaces [22], or a hemispherical bowl-shaped [23] sheath over a flat wall with an insulator/conductor interface [24] and plasma molding over a ring on a flat surface [25]. As well, plasma-surface interaction at sharp edges and corners during ion-assisted physical vapor deposition has been investigated [26,27]. All these results emphasize the important role that the geometry plays in determining the ion dose over the electrode surface.

In this paper we are reporting the three-dimensional calculation for the sheath profile and ion trajectories for disk, square, and triangle electrodes immersed in plasma. Related experiments are performed in a dc plasma using Ar gas. The results demonstrate the discrete behavior of the ion flux incident to a conducting surface that interfaces an insulator.

II. THEORETICAL CONSIDERATIONS

Let us suppose a conducting planar electrode of surface S_d biased at the potential $V_0 \ll V_{\mathrm{pl}}=0$ V, where V_{pl} is the plasma potential. The potential distribution in the sheath, $V(x,y=r,z)$ with a z axis perpendicular to the disk surface, is given by the Poisson equation,

$$\Delta V = -\frac{e}{\epsilon_0}[n_i^*(V) - n_e^*(V)]. \tag{1}$$

Assuming a Maxwellian distribution for electrons it follows that

$$n_e^*(V) = n_e \exp(-\eta_e), \tag{2}$$

where $\eta_e=-\mathrm{eV}/(kT_e)$. If the positive ions, of density n_i, are entering the sheath with c_s, then by continuity law and energy conservation one can deduce

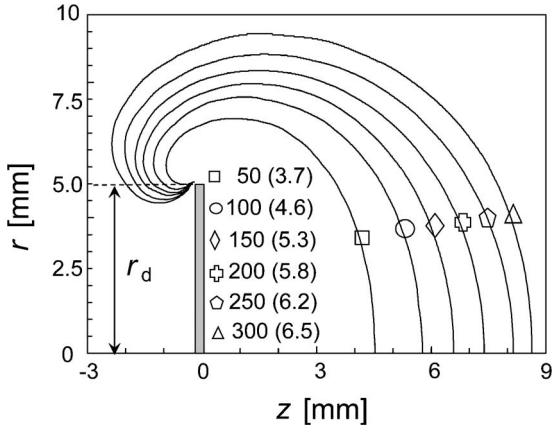

FIG. 1. Sheath edge contours of a disk electrode of radius, $r_d = 5$ mm and thickness $d = 0.2$ mm, for different values of $\eta_{e0} = \eta_e(V_0)$, where $n_i = 10^{15}$ m^{-3} and $T_e = 1$ eV. Values in brackets stand for ξ.

$$n_i^*(V) = n_i \frac{S_{sh}}{S(V)} \Psi(V), \tag{3}$$

where

$$\Psi(V) = \left(1 - \frac{2\ \text{eV}}{kT_e}\right)^{1/2}. \tag{4}$$

S is the surface of the equipotential contour given by V and S_{sh} the sheath-edge surface. Thus, Eq. (1) becomes

$$\nabla^2 V = -\frac{en_i}{\varepsilon_o}\left\{\frac{S_{sh}}{S(V)}\Psi - \exp(\eta_e)\right\}. \tag{5}$$

In practice, one can measure the electrode current I_d, which gives the current density J_d. If J_{sh} is the current density to Σ, then $S_{sh} = I_d/(en_i c_s)$. Moreover, we can introduce the current density ratio $\xi = J_d/J_{sh} = S_{sh}/S_d$. After solving Eq. (5) for various $S(V)$ dependencies we found that $S(V) = a + b\exp(\lambda V)$ with $S(V_o) = S_d$ and $S(V_{sh}) = S_{sh}$ gives the best fit to $S(V)$ obtained by solving the equation. Thus, we have

$$S(V) = S_d\left[1 + \frac{(\xi - 1)[\exp(\lambda V_o) - \exp(\lambda V)]}{\exp(\lambda V_{sh}) - \exp(\lambda V_o)}\right], \tag{6}$$

where λ is a constant coefficient. For a given ξ we iterated λ in Eq. (5) until reaching the fastest convergence of the final solution $V(x,y,z)$. The plasma-sheath boundary conditions were set as follows: $V = V_{pl}(=0)$, $\partial V/\partial x \sim \partial V/\partial y \sim \partial V/\partial z < 0.05$, and $\rho = 0$, where ρ is the total charge density.

Sheath edge contours of a disk electrode of radius $r_d = 5$ mm and thickness $d = 0.2$ mm are presented in Fig. 1 for different values of $\eta_{eo} = \eta_e(V_o)$, where $n_i = 10^{15}$ m^{-3} and $T_e = 1$ eV. Values in brackets stand for ξ. The flat disk surface facing z direction and the lateral side were biased to V_o (conductor) while the side facing $-z$ to $V = V_f$ (insulator). Here, for simplicity, since $V_o \ll V_{pl}$ we neglected the floating potential, V_f, setting $V_f = 0$. Even for $\eta_{e0} = 50$, the sheath edge exhibited a mushroomlike structure that expanded by increasing η_{e0}, reaching the sheath thickness $D \sim 2r_d$ for $\eta_{e0} = 300$. Since both sides of the disk were exposed to plasma, the sheath also expanded in the $-z$ direction. $\eta_e(0,0,z)$ by Eq. (5) for $r_d = 5$ mm is presented in Fig. 2(a) with solid lines for three values of η_{e0} while $\eta_e(0,0,z)$ for $r_d = 100$ mm (infinitelike electrode) is shown with dashed lines. $\eta_e(0,0,z)$ for similar values of r_d but different n_i is presented in Fig. 2(b), where $\eta_{e0} = 150$ and $T_e = 1$ eV. Thus, besides n_e, T_e, and V_0, the sheath expansion and its shape depends on r_d. If R is the curvature radius of Σ obtained for $x = 0$ and $r = 0$, then the ratios R/D and $D/(2r_d)$ gives information about the shape of the sheath-edge front. For instance, R/D and $D/(2r_d)$ related to the sheath profiles shown in Fig. 2(b) are presented in Table I. At low density ($n_i = 10^{14}$ m^{-3}) D exceeded $2r_d$ while the sheath front remained almost spherical with $R \cong D$. For $n_i > 10^{16}$ m^{-3} we found $R \gg D$ and $D/(2r_d) < 1$, so that the

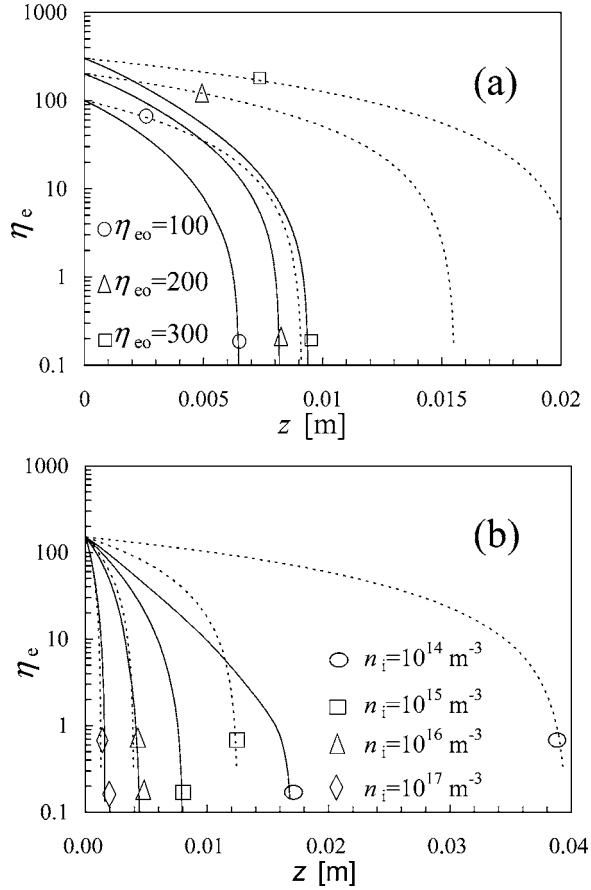

FIG. 2. (a) $\eta_e(0,0,z)$ by Eq. (5) for three values of η_{e0} with solid lines for $r_d = 5$ mm and with dashed lines for $r_d = 100$ mm (infinitelike electrode); (b) $\eta_e(0,0,z)$ for similar values of r_d but different n_i. In both figures, $T_e = 1$ eV.

TABLE I. R/D and $D/(2r_d)$ related to the sheath profiles shown in Fig. 2(b).

n_i (m^{-3})	R/D	$D/(2r_d)$
10^{14}	1.07	1.21
10^{15}	1.69	0.79
10^{16}	3.8	0.23
10^{17}	20	0.15

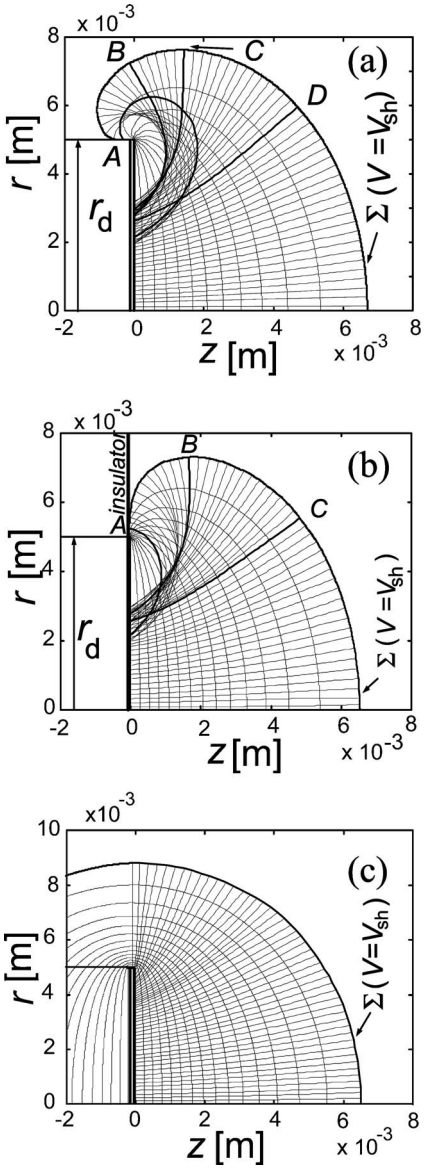

FIG. 3. Potential distribution, as equipotential contours, and ion trajectories starting from the sheath edge until reaching the surface: (a) for a one-side-biased disk; (b) a biased-disk extended on its plane by an insulator; (c) a both-side-biased disk. In all simulations we set $\eta_{e0}=150$, $n_i=10^{15}$ m^{-3}, $T_e=1$ eV, and $\xi=9$ for (a) $\xi=9.7$ for (b), and $\xi=9.3$ for (c).

sheath expanded as much as for an infinite electrode.

The potential distribution, as equipotential contours, and ion trajectories starting from the sheath edge until reaching the surface, are presented in Fig. 3 for a one-side-biased disk (a); a biased disk extended on its plane by an insulator (b); a both-side-biased disk (c), respectively, where $\eta_{e0}=150$, $n_i=10^{15}$ m^{-3}, $T_e=1$ eV, and $\xi=9$ for (a), $\xi=9.7$ for (b), and $\xi=9.3$ for (c). In order to account for the presheath, the initial ion velocity at the sheath edge was set to c_s with an orientation perpendicular to Σ. Let (x_0, y_0, z_0) be the coordinates of a positive ion on the sheath edge, and $(\nu_{0x}, \nu_{0y}, \nu_{0z})$ the ion velocity in a thin layer of the sheath delineated by $V_{sh} > V > V^*$, where V^* is less than 1% of V_0, so that we can define ions with $z_0 < 0$ as back side ions and ions with $z_0 \geqslant$ as

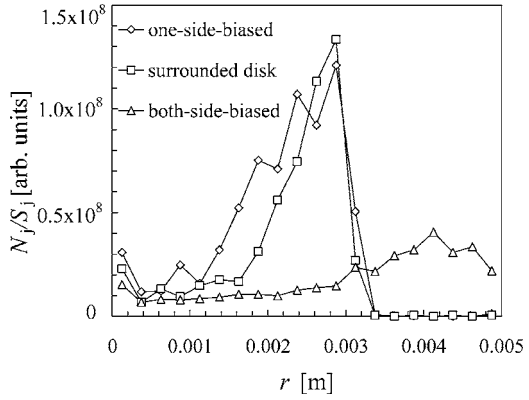

FIG. 4. N_j/S_j as a function of r for electrodes shown in Fig. 3, where $N=2000$.

frontal ions. In Fig. 3(a) the back side ions (from A to B) were first accelerated in the z direction to finally reach the central part of the surface coming from the $-z$ direction (oblique incidence). The frontal ions from B to D were all focalized to a narrow part on the disk surface, leading to the formation of an area of no ion impact, named passive surface (PS), between the electrode edge and the focalization region. The location C marks the change from $\nu_{0z} > 0$ to $\nu_{0z} < 0$. Trajectories from D to the disk center ($r=0$) exhibited a reduced curvature, so that ions reached the surface under higher incidence angles, α_{imp}, with $\alpha_{imp}=90$ deg for $r=0$. If r_{imp} is defined as the location delineating PS from the region of ion impact, it follows that r_{imp} depends on plasma parameters, r_d and V_0. By extending the disk on its plane with an insulator (see Fig. 3(b)), the sheath expansion was restricted to $z_0 \geqslant 0$ (only frontal ions). However, since from A to B the ions entered the sheath with $\nu_{z0} > 0$, their trajectories exhibited a higher curvature that also led to the formation of PS, as previously shown in Fig. 3(a). Moreover, from B to C and C to $z=0$ the ions trajectories were almost similar with those from C to D and D to center in Fig. 3(a). For a both-side-biased disk (see Fig. 3(c)) all ions have shown $\nu_{z0} \leqslant 0$ for $z_0 > 0$, thus no PS was formed, the entire surface being reached by ions with a slight increase of the ion dose near the edge. In practice, the incident ion flux on the electrode surface induces various surface reactions, some of which show angular dependence, so that the reveled change of α_{imp} with r that one can notice from Fig. 3 is an important factor in plasma processing.

Let us divide S_d in $j=1\cdots20$ concentric elements, S_j, and assume a total number, N, of test ions that enter the sheath from certain locations uniformly distributed on Σ. If N_j is the number of test ions reaching each S_j, then the ratio N_j/S_j is proportional to the ion current density. N_j/S_j as a function of r for electrodes shown in Fig. 3 is presented in Fig. 4, where $N=2000$. Thus, more than 50% of the ions entering the sheath have been focused to less than 15% of the electrode area leading to the formation of a distinctive ringlike region on the electrodes surfaces that interfaced insulators, Figs. 3(a) and 3(b), respectively. In the case of a both-side-biased disk the ion current density was peaked near to, but not on, the edge, as previously reported [13].

The impact locations on the surface of an one-side-conducting disk of 2000 ions passing through the sheath ob-

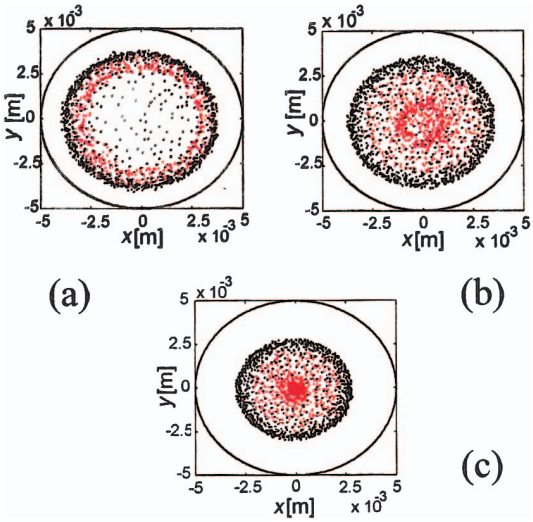

FIG. 5. (Color) The impact locations on the surface of a one-side-conducting disk of 2000 ions passing through the sheath obtained by applying $V_0=-100$, -200, and -300 V ($n_i=10^{15}$ m^{-3}, $r_d=5$ mm and $T_e=1$ eV) respectively, where the back side ions were represented with red dots and the frontal ions with black dots.

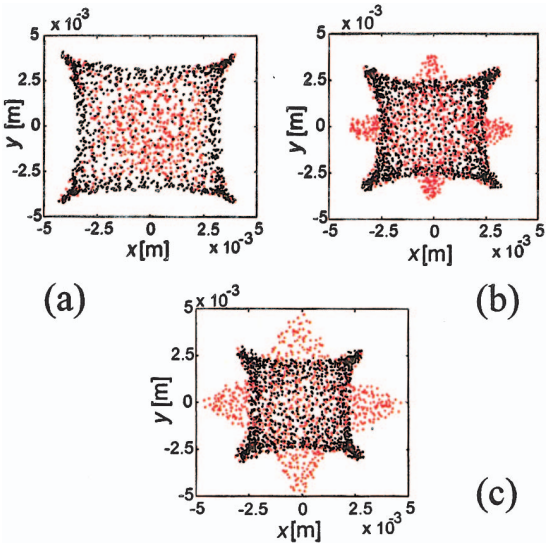

FIG. 6. (Color) The impact location of ions on the surface of square electrodes for (a) $V_0=-100$ V; (b) -200 V; and (c) -300 V, where $l_d=10$ mm, $n_i=10^{15}$ m^{-3}, and $T_e=1$ eV. The back side ions are represented with red dots and frontal ions with black dots.

tained by applying $V_0=-100$, -200, and -300 V ($n_i=10^{15}$ m^{-3}, $r_d=5$ mm, and $T_e=1$ eV) are shown in Figs. 5(a)–5(c), respectively, where the back side ions were represented with red dots and the frontal ions with black dots. Thus, the PS delineation from the active surface was very sharp, clearly showing the formation by frontal ions of the ringlike region of which radius, and implicitly r_{imp}, decreased by decreasing V_0. Quite unexpected was the behavior of the back side ions. Based on the spherical profile of the sheath front at very low V_0 (see Table I), it was expected that the focusing of the frontal ions will take place at the electrode center [16,20]. Even that a small increasing of the frontal-ion flux at the center have been previously reported [19], present results shows that the spotlike structure was formed at the electrode center through focusing of the back side ions. For instance, no central spot was formed when applying $V_0=-300$ V to the disk extended on its plane by an insulator (see Fig. 3(b)) and ion impact locations resembled closely the image from Fig. 3(c), except for the presence of the red dots. When considering square electrodes of $l_d=10$ mm in length, the impact location of ions on the surface becomes more complex, as can be seen from Fig. 6, where simulations for similar parameters as those used in Fig. 5 are presented [$n_i=10^{15}$ m^{-3}, $T_e=1$ eV, and $V_0=-100$, -200, and -300 V corresponding to (a), (b), and (c), respectively]. The back side ions are represented with red dots and frontal ions with black dots. While the impact area of frontal ions decreased by decreasing V_0, that of the back side ions increased, eventually exceeding the profile delineated by frontal ions. The corners forming the starlike profile corresponding to frontal ions were very sharp and included a large number of ions while the profile resulted by back side ions was very complex, exhibiting modal lines and modal spots, as we reported recently [28].

III. EXPERIMENTAL RESULTS

Experiments were performed in a cylindrical device of 250 mm in diameter and 300 mm in length. The lateral surface of the chamber was covered on the outer side with permanent magnets that reduced the wall losses. A low-density plasma, $n_i<5\times10^{16}$ m^{-3}, was produced by dc discharge using a directly heated filament. The discharge bias, U_{ac}, of 100 V was applied between the filament as a cathode and the grounded wall as an anode. By adjusting the filament current we could control the discharge current, I_{ac} and, respectively, control n_i. All measurements were performed in Ar gas. Electrodes of different shapes (i.e., disk, square, and triangle) were made of gold, silver, and brass (plate of 0.2 mm in thickness), materials that have a high sputtering yield by Ar^+ bombardment and exhibit a good visibility of the sputtered patterns. Depending on the scope, the electrodes were both side conductive, one-side insulated with a layer of ceramic cement (less than 1 mm), or fixed on the surface of a large ceramic plate, (0.5 mm thick, and $4r_d$ in diameter for disks and $3l_d$ in length for squares). The electrodes were biased with $V_0 \ll V_{pl}$ for a time, t, while measuring the flowing current I_d. A cylindrical probe was used to detect the plasma parameters and to monitor eventual changes during the electrode biasing [29]. Photographs of disk, square, and triangle electrodes exposed to plasma for $t=3$ min, $n_i \cong 10^{15}$ m^{-3}, and $T_e=1.7$ eV are shown in Fig. 7 for $V_0=-100$ V, (a), (d), and (g); -200 V (b), (e), and (h); and -300 V (c), (f), and (i), respectively. All pictures show a dark region near the edge, corresponding to PS, and a bright region of nonuniform contrast corresponding to the active surface. Comparing simulations presented in Fig. 5 with photographs of disk electrodes from Fig. 7, one can find a very good agreement in terms of r_{imp} values and their dependence on V_0. Moreover, the prediction that the back side ions will be focused to a spot at the disk center for $V_0 \leqslant 200$ V was correct. For square elec-

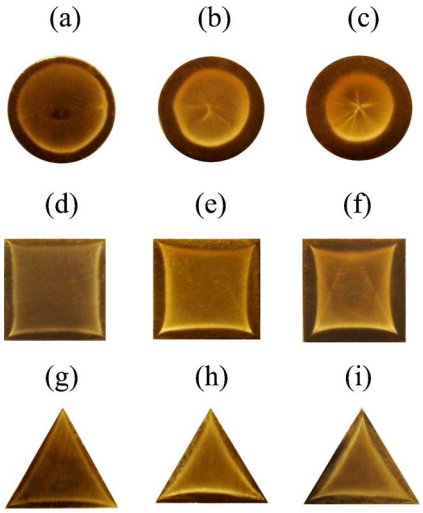

FIG. 7. (Color online) Photographs of disk, square, and triangle electrodes exposed to plasma for $t=3$ min, $n_i \cong 10^{15}$ m^{-3}, and $T_e=1.7$ eV. (a), (d), and (g) for $V_0=-100$ V; (b), (e), and (h) for $V_0=-200$ V; and (c), (f), and (i) for $V_0=-300$ V, respectively.

trodes, the intense sputtering by frontal ions resulted in a starlike pattern of which the area decreased with decreasing V_0. The triangle electrodes show a similar discrete focusing effect by forming a PS of an area that also increased with decreasing V_0. Paying attention to details, one can notice from Figs. 7(b) and 7(c) that the spot exhibits an irregular structure, including certain preferential radial directions, randomly distributed but converging at the disk center. Some fine lines, passing over the active surface of the square electrode, are also visible in Fig. 7(f). The origin of these lines (named "modal lines") was recently clarified for electrodes with sharp corners [28]. However, details about the spot structure for disk electrodes remained unexplained. For instance, photographs of two electrodes, made of brass, treated simultaneously for $t=60$ min, $V_0=-500$ V, $n_i=5\times10^{15}$ m^{-3}, $T_e=1.6$ eV, $r_d=6$ mm are shown in Fig. 8, where (a) corresponds to a one-side-biased disk and (b) to a one-side-biased dodecagon. Even that both electrodes exhibited modal lines, those of the disk were irregular while those of the dodecagon were correlated with respect to the corners. This fact proves that any small irregularity on the edge of the disk (the structure, metallic-plate-cement layer was not geometrically perfect) mostly affected the part of the sheath expanding in the

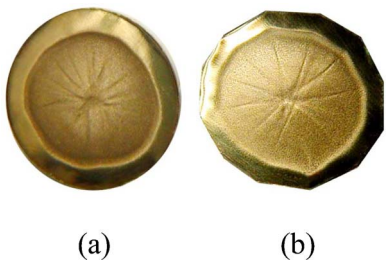

FIG. 8. (Color online) Photographs of two electrodes, made of brass, treated simultaneously for $t=60$ min, $V_0=-500$ V, $n_i=5\times10^{15}$ m^{-3}, $T_e=1.6$ eV, and $r_d=6$ mm. (a) One-side-biased disk; (b) one-side-biased dodecagon.

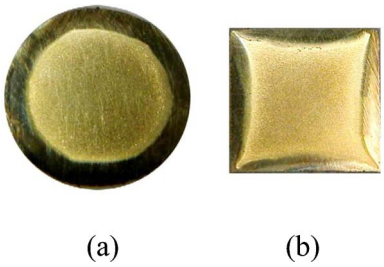

FIG. 9. (Color online) Photographs of (a) a disk ($r_d=6$ mm) and (b) a square electrode ($l_d=10$ mm), made of brass and surrounded by insulating plates of ceramic, after having been treated simultaneously in Ar plasma for $t=60$ min, $V_0=-300$ V, $n_i=10^{15}$ m^{-3}, and $T_e=1.7$ eV.

−z direction, leading to preferential directions of focalization. It also suggests that it make sense to consider a well-defined Σ that can follow in detail the potential distribution within the sheath.

As shown in Fig. 3(b), the introduction of an insulator in the $z=0$ plane restricted the sheath expansion in the −z direction, so that the absence of the back side ions should lead to the absence of the spot for disk electrodes or modal lines for electrodes with sharp corners. Photographs of a disk ($r_d=6$ mm) and a square electrode ($l_d=10$ mm) surrounded by insulating plates made of ceramic cement are shown in Figs. 9(a) and 9(b), respectively, after being treated simultaneously in Ar plasma for $t=60$ min, $V_0=-300$ V, $n_i=10^{15}$ m^{-3}, and $T_e=1.7$ eV. Both electrodes show very well-defined PS with no evidence of any central spot or modal lines. It is important to notice that irregularities in the interface between the electrode and the ceramic cement were actually amplified on the contour delineating PS from the active surface.

Surface modification by focalized positive ions was previously reported using SEM or AFM images [18,19,28]. In the present work we emphasize the difference given by the presence or absence of an insulating material adjacent to the electrode. Thus, the simulation results presented in Fig. 3 and Fig. 4 were reproduced experimentally by using three disk electrodes ($r_d=5$ mm) made of silver plate, 0.2 mm in thickness, that have been exposed to Ar plasma for $t=30$ min, $V_0=-300$ V, $n_i=10^{15}$ m^{-3}, and $T_e=1.6$ eV. The R_{rms} of these samples, measured by AFM, for 10×10 μm^2 with a radial resolution of 0.25 mm is presented in Fig. 10. From simulations it resulted that α_{imp} was larger on the intense sputtered ring comparatively to the central part of the electrode, a fact that can increase the sputtering yield at that particular location. Keeping in mind this observation we can conclude that the ion flux distribution presented in Fig. 4 agrees very well with R_{rms} results presented in Fig. 10.

A reliable evaluation of D for electrodes of about one cm in diameter is quite a difficult task. Moreover, the plasma-presheath-sheath debate, including a definite criterion for the sheath edge, is yet animating the scientific community, even for the one-dimensional case (see, for instance, Ref. [2] and the comments following it). In order to cross-check the values of D obtained by simulations with some experimental measurements, we built the setup shown in Fig. 11, where the central part of an electrode (2 mm in diameter) was sepa-

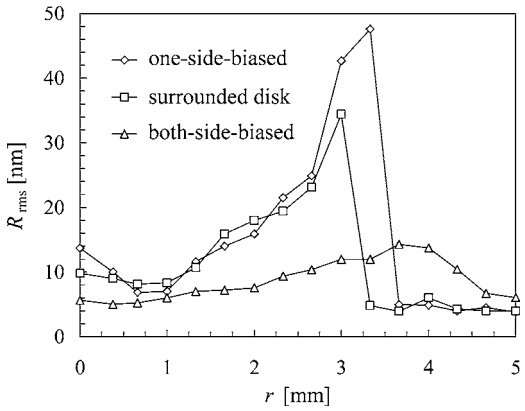

FIG. 10. The R_{rms} measured by AFM, for 10×10 μm^2 with a radial resolution of 0.25 mm for different disk electrodes (r_d =5 mm) made of silver plate, 0.2 mm in thickness, that have been exposed to Ar plasma for t=30 min, V_0=−300 V, $n_i=10^{15}$ m^{-3}, and T_e=1.6 eV.

rated by a gap of 0.3 mm from the total disk structure of 10 mm in diameter. The back side of the two parts was covered with ceramic cement; both electrodes being biased to V_0. A small probe of 0.1 mm in diameter and 2 mm in length was supported by a ceramic tube of 0.5 mm in diameter and moved by a motor in the z direction while keeping its bias at plasma potential and measuring the current, I_e. I_e as a function of z for different values of V_0 is presented in Fig. 12, where $n_i=10^{15}$ m^{-3}, p=3 m Torr, and T_e=1.6 eV. D corresponding to Fig. 1 is shown by vertical lines. As one can see, simulations predicted a D that matches well the beginning of the transition from a flat I_e to an accentuated decreasing due to electron reflection. It is remarkable that D from simulation shows a similar dependence with V_0 as that resulting from measurement if one arbitrarily decides the sheath edge at a location where I_e decreases with a factor of 2 with respect to its value in plasma.

IV. CONCLUSIONS

The positive-ion flux distribution on the surface of biased electrodes of different geometries immersed in plasma was

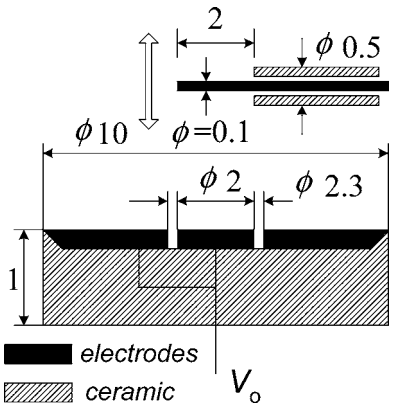

FIG. 11. The setup used to measure the electronic current in the sheath, where all dimensions are in mm.

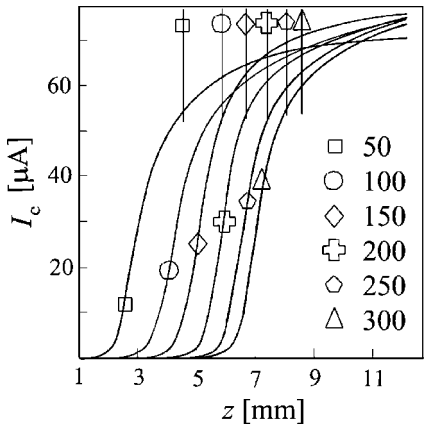

FIG. 12. I_e as a function of z for different values of V_0, where $n_i=10^{15}$ m^{-3}, p=3 m Torr, and T_e=1.6 eV. Vertical lines correspond to D from Fig. 1.

investigated by three-dimensional simulations and experiments. It was demonstrated that the sheath surrounding electrodes that have interfaced insulators acted as an electrostatic lens, focusing the positive ions to distinct locations on the electrode surface. Depending on the entrance coordinates in the sheath, positive ions have been divided in frontal ions ($z_o \geqslant 0$) and back side ions ($z_o < 0$). Since their kinetic within the sheath was different, the focusing effect involving frontal ions was defined as discrete focusing and the focusing effect involving back side ions as modal focusing [28]. The discrete focusing led to the formation of a passive surface (PS), of no ion impact, near the edge of the electrode interfacing insulators. The PS shape and its area were dependent on the electrode shape and plasma parameters. The modal focusing leaded to the formation of certain "modal spots" and/or "modal lines" that have been investigated in detail elsewhere [28]. There are several reasons why these focusing effects have been treated separately. Thus, by choosing an appropriate conductor-insulator interface the discrete focusing could be produced independently from the modal focusing. While the discrete focusing exhibited a very well-defined boundary between the PS and AS, by a high ion flux, the modal focusing only resulted in a diffuse delineation. The impact angles of ions producing the discrete focusing were significantly higher than those of modal ions, obviously inducing different surface modifications. For some geometries, for instance square electrodes, the area ratio PS/AS showed a reversed dependence when decreasing the applied bias, increasing for discrete focusing and decreasing for modal focusing.

Beside some applications that have already been proposed [18,19], it is expected that the sheath lens focusing effects will impact some other aspects related to plasma processing [30] and surface modification by developing a complex 3D sheath lens able to control the ion flux in a desired manner.

ACKNOWLEDGMENT

This work was partially supported by the 21st Century Center of Excellence Program of the Ministry of Education, Culture, Sports, Science, and Technology, Japan.

[1] I. Langmuir, Phys. Rev. **33**, 954 (1929).
[2] V. Godyak and N. Stemberg, Phys. Plasmas **9**, 4427 (2002).
[3] R. N. Franklin and J. Snell, Phys. Plasmas **8**, 643 (2001).
[4] K.-U. Riemann and L. Tsendin, J. Appl. Phys. **90**, 5487 (2001).
[5] V. Vahedi, R. A. Stewart, and M. A. Lieberman, J. Vac. Sci. Technol. A **11**, 1275 (1993).
[6] A. Kono, Phys. Plasmas **10**, 4181 (2003).
[7] D. Bohm, *The Characteristics of Electrical Discharges in Magnetic Fields*, edited by A. Guthrie and R. K. Wakerlink (McGraw-Hill, New York, 1949), Chap. 3.
[8] M. A. Lieberman and A. J. Lichtenberg, *Principles of Plasma Discharges and Material Processing* (Wiley, New York, 1994).
[9] J. R. Conrad, J. Appl. Phys. **62**, 777 (1987).
[10] I. J. Donnelly and P. A. Watterson, J. Phys. D **22**, 90 (1989).
[11] P. A. Watterson, J. Phys. D **22**, 1300 (1989).
[12] M. Hong and G. A. Emmert, J. Appl. Phys. **78**, 6967 (1995).
[13] T. E. Sheridan, Appl. Phys. Lett. **68**, 1918 (1996).
[14] M. Paulus, L. Stals, U. Rude, and B. Rauschenbach, J. Appl. Phys. **85**, 761 (1999).
[15] Z. Fan, P. K. Chu, C. Chan and N. W. Cheung, Appl. Phys. Lett. **73**, 202 (1998).
[16] E. Stamate and K. Ohe, Appl. Phys. Lett. **78**, 153 (2001).
[17] E. Stamate and K. Ohe, J. Vac. Sci. Technol. A **20**, 661 (2002).
[18] E. Stamate, K. Ohe, O. Takai, and H. Sugai, Surf. Coat. Technol. **169–170**, 65 (2003).
[19] E. Stamate, H. Sugai, O. Takai, and K. Ohe, J. Appl. Phys. **95**, 830 (2004).
[20] X. B. Tian and P. K. Chu, Appl. Phys. Lett. **81**, 3744 (2002).
[21] O. Demokan, J. Appl. Phys. **91**, 5587 (2002).
[22] B. Briehl and H. M. Urbassek, J. Appl. Phys. **93**, 4420 (2003).
[23] C. Liu and D. Wang, Surf. Coat. Technol. **171**, 119 (2003).
[24] D. Kim and D. Economu, J. Appl. Phys. **94**, 2852 (2003).
[25] D. Kim and D. Economu, J. Appl. Phys. **94**, 3740 (2003).
[26] E. B. Macak, W. D. Munz, and J. M. Rodenburg, J. Appl. Phys. **94**, 2829 (2003).
[27] E. B. Macak, W. D. Munz, and J. M. Rodenburg, J. Appl. Phys. **94**, 2837 (2003).
[28] E. Stamate and H. Sugai, Phys. Rev. Lett. **94**, 125004 (2005).
[29] E. Stamate, G. Popa, and K. Ohe, Rev. Sci. Instrum. **70**, 58 (1999).
[30] E. Stamate, N. Holtzer, and H. Sugai, Appl. Phys. Lett. **86**, 261501 (2005).